

Coastal Flooding in Florida's Big Bend Region with Application to Sea Level Rise Based on Synthetic Storms Analysis

Scott C. Hagen^{1,*} and Peter Bacopoulos²

¹Department of Civil, Environmental, and Construction Engineering, University of Central Florida, Orlando, Florida, USA

²Taylor Engineering Research Institute, School of Engineering, University of North Florida, Jacksonville, Florida, USA

Received 30 September 2011, accepted 17 April 2012

ABSTRACT

Flooding is examined by comparing maximum envelopes of water against the 0.2% (= 1-in-500-year return-period) flooding surface generated as part of revising the Federal Emergency Management Agency's flood insurance rate maps for Franklin, Wakulla, and Jefferson counties in Florida's Big Bend Region. The analysis condenses the number of storms to a small fraction of the original 159 used in production. The analysis is performed by assessing which synthetic storms contributed to inundation extent (the extent of inundation into the floodplain), coverage (the overall surface area of the inundated floodplain) and the spatially variable 0.2% flooding surface. The results are interpreted in terms of storm attributes (pressure deficit, radius to maximum winds, translation speed, storm heading, and landfall location) and the physical processes occurring within the natural system (storms surge and waves); both are contextualized against existing and new hurricane scales. The approach identifies what types of storms and storm attributes lead to what types of inundation, as measured in terms of extent and coverage, in Florida's Big Bend Region and provides a basis in the identification of a select subset of synthetic storms for studying the impact of sea level rise. The sea level rise application provides a clear contrast between a dynamic approach versus that of a static approach.

Key words: Storm surge, Waves, Floodplain inundation, Hurricane scales, Climate change

Citation: Hagen, S. C. and P. Bacopoulos, 2012: Coastal flooding in Florida's Big Bend Region with application to sea level rise based on synthetic storms analysis. *Terr. Atmos. Ocean. Sci.*, 23, 481-500, doi: 10.3319/TAO.2012.04.17.01(WMH)

1. EXISTING AND NEW HURRICANE SCALE(S)

1.1 Saffir-Simpson Hurricane Scale

The Saffir-Simpson Hurricane Scale (SSHS) was introduced in the 1970s to provide a means for estimating expected hurricane wind damages (Simpson 1974). The SSHS (Table 1) has been used extensively for hurricane evacuation preparations and emergency response planning; however, there are respectable criticisms on the SSHS: (i) the scale is quantized, i.e., each hurricane category has a range of properties assigned to it and it saturates at the higher end, i.e., it is capped at Category 5 (Kantha 2006); (ii) the scale omits the influence of hurricane size (Powell and Reinhold 2007; Irish et al. 2008; Kantha 2008); and (iii) the scale does not account for other important factors directly influencing surge generation, e.g., regional bathymetry (Irish and Resio 2010). Suggestions for improvements of the SSHS are

Table 1. The Saffir-Simpson Hurricane Scale.

Storm type	Minimum central pressure (hPa)	Maximum sustained winds (m s ⁻¹)
Tropical depression	1007	< 17
Tropical storm	< 1000	17 - 33
Hurricane		
Category 1	980	33 - 42
Category 2	979 - 965	43 - 49
Category 3	964 - 945	50 - 58
Category 4	944 - 920	59 - 69
Category 5	< 920	> 70

* Corresponding author
E-mail: scott.hagen@ucf.edu

centered on the common theme of incorporating additional influencing factors as they relate to both hurricane wind damage and storm surge flooding damage.

1.2 Hurricane Intensity Index and Hurricane Hazard Index

The Hurricane Intensity Index (HII) uses maximum sustained near-surface wind speed V_{\max} as the dependent parameter:

$$\text{HII} = \left(\frac{V_{\max}}{V_{\max,0}} \right)^2 \quad (1)$$

where HII is the dimensionless Hurricane Intensity Index, V_{\max} is the maximum sustained near-surface wind speed in m s^{-1} , and the subscript 0 stands for the reference value. The

HII can be considered a guidance tool for evacuation preparations prior to landfall in that it directly accounts for hurricane intensity, viz. Eq. (1): $\text{HII} \sim V_{\max}^2$.

However, the HII does not account for other important storm attributes and measures Hurricane Katrina as $\text{HII} = 3.0$ and Hurricane Andrew as $\text{HII} = 5.2$ (Table 2) when in fact, Hurricane Katrina was much more destructive than Hurricane Andrew. In this comparison, storm size becomes a contributing factor (Irish et al. 2008) in that Hurricane Katrina was almost twice the size of Hurricane Andrew. Emanuel (2005) pointed out that total energy dissipation rate in storms scales like the cube of the wind speed, as does the monetary loss. The hazard also depends on the residence time of the hurricane. DeVised on the basis of maximum sustained near-surface wind speed V_{\max} (a proxy of intensity), radius to maximum winds R_{\max} (a proxy of storm size), and translational speed of the storm S (a proxy of residence time), the Hurricane Hazard Index (HHI) is given as:

Table 2. Attributes and categorizations of select historical hurricanes and top 7 contributing storms. Estimates of HII [Eq. (1)] and HHI [Eq. (2)] are based on $V_{\max,0} = 33 \text{ m s}^{-1}$ (equivalent to Cat 1 on SSHS), $R_{\max,0} = 54 \text{ km}$ (30 mi), and $S_0 = 6.7 \text{ m s}^{-1}$ (15 mph).

Select historical hurricanes										
Storm name	ΔP^a (hPa)	$V_{\max}^{b,d}$ (m s^{-1})	$R_{\max}^{c,d}$ (km)	S^e (m s^{-1})	SSHS ^{f,g}	HII ^h	HHI ⁱ	Storm angle ^j (deg)	Storm landfall	
									(°W)	(°N)
Andrew	64	68	19		Cat 5	5.2	11.9			
Opal	73	50	98		Cat 3	2.4	8.2			
Ivan	58	49	35		Cat 3	2.7	7.4			
Dennis	61	51	9		Cat 3	2.7	1.9			
Katrina	94	52	65		Cat 3	3.0	14.6			
Rita	67	49	30		Cat 3	2.4	8.4			
Wilma	62	51	72		Cat 3	2.5	9.2			
Top 7 contributing storms										
Storm number	ΔP^a (hPa)	$V_{\max}^{b,d}$ (m s^{-1})	$R_{\max}^{c,d}$ (km)	S^e (m s^{-1})	SSHS ^{f,g}	HII ^h	HHI ⁱ	Storm angle ^j (deg)	Storm landfall	
									(°W)	(°N)
85	87	69	37	6.8	Cat 4	4.3	4.2	+28	84.72	29.81
84	87	69	37	6.8	Cat 4	4.3	4.2	+28	85.20	29.75
83	87	69	37	6.8	Cat 4	4.3	4.2	+28	85.53	29.93
65	56	57	68	4.2	Cat 3	3.0	13.3	+61	85.01	29.73
64	56	57	68	4.2	Cat 3	3.0	13.3	+61	85.72	30.08
86	87	69	37	6.8	Cat 4	4.3	4.2	+28	84.19	29.94
82	87	69	37	6.8	Cat 4	4.3	4.2	+28	85.83	30.15

^a ΔP = pressure deficit, historical values from National Hurricane Center (2012).

^b V_{\max} = maximum sustained near-surface wind speed; synthetic values estimated using Table 1.

^c R_{\max} = radius to maximum winds.

^d Historical values from Powell and Reinhold (2007).

^e Translational speed.

^f SSHS = Saffir-Simpson Hurricane Scale at time of landfall.

^g Historical values from Blake et al. (2011).

^h HII = Hurricane Intensity Index; historical values from Powell and Reinhold (2007).

ⁱ HHI = Hurricane Hazard Index; historical values from Kantha (2008).

^j Degree measures are clockwise from true north.

$$\text{HHI} = \left(\frac{V_{\max}}{V_{\max,0}} \right)^3 \left(\frac{R_{\max}}{R_{\max,0}} \right)^2 \left(\frac{S_0}{S} \right) \quad (2)$$

where HHI is the dimensionless Hurricane Hazard Index, V_{\max} is the maximum sustained near-surface wind speed in m s^{-1} , R_{\max} is the radius to maximum winds in km, S is the translational speed of the storm in m s^{-1} , and the subscripts 0 stand for reference values. The HHI can be considered a guidance tool for emergency planners in the aftermath of the storm in that it directly accounts for the hurricane hazard, viz. Eq. (2): $\text{HHI} \sim (V_{\max}^3)(R_{\max}^2)(S^{-1})$. Referring to Table 2, Hurricane Andrew with a landfall wind speed of 74 m s^{-1} (165 mph) but radius to maximum winds of only 97 km (60 mi) measures as $\text{HHI} = 11.9$ (Landsea et al. 2004), and (125 mph) and radius to maximum winds of 193 km (120 mi) measures as $\text{HHI} = 14.6$ (Knabb et al. 2005). In this comparison, the HHI is more reflective of the hazard potential than is the SSHS.

1.3 Surge Response Function Approach

Resio et al. (2009) developed a surge response function approach, a variant of the standard Joint Probability Method (JPM) approach to coastal hazard assessment. A basic concept of the approach is to maximize the information content in the sample set of storms to be simulated and introduced into the JPM surge matrices. The probabilistic basis is capable of generating statistical flooding surfaces, e.g., the 1% (= 1-in-100-year return-period) flooding surfaces, with high fidelity and efficient computation. Irish et al. (2009) quantify the spatial attributes associated with the surge response function approach as applied for the Texas, USA coastline. They call “for [a] more comprehensive application in hurricane surge studies, the response functions developed here should be expanded to include the impacts of other physical processes such as storm angle of approach and translational speed, wave setup, inland runoff, and locally generated wind setup.” [Irish et al. (2009), p. 204]. The methodology presented in this paper accounts for these additional physical processes with the exception of inland runoff.

2. SEA LEVEL RISE IMPACT

Sea level rise is an indicator of climate change which can have significant effects on the coastal environment with one such effect coming in the form of increased flooding (Parker 1991). The response in coastal flooding due to sea level rise can be linear or nonlinear. The linear response is analogous to a static response, which means that existing dynamics will simply be elevated by the amount of sea level rise. As an example, if the existing flooding extent is located at the 10-m topographic contour, then the static approach applies the amount of sea level rise directly to this existing measure and forecasts the future (sea level rise = 0.5 m)

flooding extent to be located at the 10.5-m topographic contour. The linear nature here is that no dynamic interaction occurs and the perturbation X into the system leads to the response X within the system. The nonlinear response is analogous to a dynamic response, which means that future dynamics occur in the face of sea level rise. The dynamic approach accounts for nonlinear effects, e.g., an increased sea level of 0.5 m might lead to a greater or lesser increase ($+0.5 \text{ m} \pm \Delta_{\text{nonlinear}} \text{ m}$) in topographic elevation of flooding extent where the future flooding extent with sea level rise of 0.5 m is forecast to be located at the $10.5 \pm \Delta_{\text{nonlinear}}$ -m topographic contour. While an additive or subtractive nonlinear response $\Delta_{\text{nonlinear}}$ could be considered a small measure, it is important to account for the fact that with flat topography, small vertical increases could lead to expansive spatial impacts. The dynamic approach applied herein is expected to draw out any such instances of nonlinear response.

3. PRODUCTION RUNS, MAXIMUM ENVELOPES OF WATER (MEOWS), AND 500-YEAR FLOODPLAIN

Production runs were performed using the ADvanced CIRCulation (ADCIRC) numerical code (Luettich and Westerink 2006) and Simulating Waves Nearshore (SWAN) numerical code (SWAN Team 2010). Output included maximum envelopes of water (MEOWs), which are worst-case snapshots of flooding extent resulting from given storms, for Franklin, Wakulla, and Jefferson counties in Florida’s Big Bend Region [see the National Hurricane Center (2011a) for a definition]. The ADCIRC model domain employed a version of the Western North Atlantic Tidal model domain which hones in on Franklin, Wakulla, and Jefferson counties located in the northeastern Gulf of Mexico (Hagen et al. 2006) (Fig. 1). The large-scale, unstructured finite element (ADCIRC) mesh was designed to extend deeply into Franklin, Wakulla, and Jefferson counties (Salisbury et al. 2011). The SWAN model domain was designed in a nested fashion honing in on Florida’s Big Bend Region (Slinn et al. 2011). The ADCIRC and SWAN model domains focus on Franklin, Wakulla, and Jefferson counties but also cover two adjacent coastal counties, Gulf and Taylor. The extension of the model domains into Gulf and Taylor counties ensured a full set of 159 storm surge simulations over Gulf and Taylor counties and into Franklin, Wakulla, and Jefferson counties would be properly accounted for and not artificially prohibited by an imposed no-flow boundary.

There has been rigorous validation using these same exact models (ADCIRC and SWAN) of the study site, noting that the validation exercise exhausted the observational data available in the region regarding historical storm surge events. The validation of the ADCIRC and SWAN models is demonstrated by Atkinson et al. (2011) and Slinn et al. (2011), respectively.

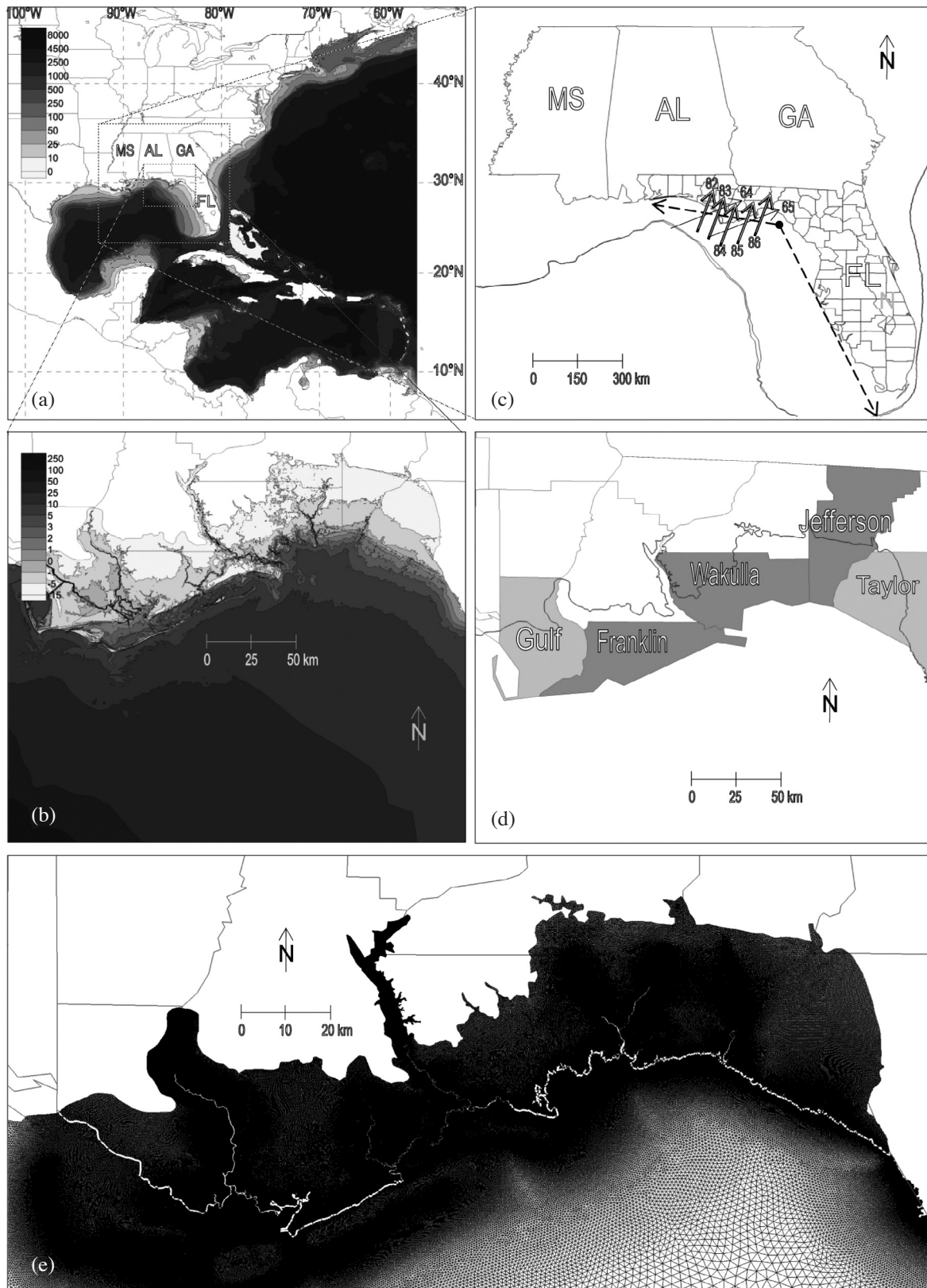


Fig. 1. Bathymetry/topography (m, North American Vertical Datum of 1988) of (a) Western North Atlantic Tidal model domain and (b) Florida's Big Bend Region. (c) Landfall locations and local storm tracks (arrow length = $2 \times$ radius to maximum winds; \longrightarrow = ≈ 45 hPa pressure deficit; and \longleftarrow = ≈ 90 hPa pressure deficit) for 7 contributing storms (numbered). Continental shelf break: 183- and 200-m depth contours (===). Approximation of coastline angle ($\longleftarrow \bullet \longrightarrow$). (d) Franklin, Wakulla, and Jefferson (■) and Gulf and Taylor (▨) counties and ADCIRC model boundary (—). (e) ADCIRC mesh and zero-elevation contour (—) as seaward boundary of a defined floodplain. MS = Mississippi, AL = Alabama, GA = Georgia, and FL = Florida.

A total of 159 storms were used in production to encompass a wide range of inundation hazards. The 159 storms include synthetic tropical storms and hurricanes (landfall and bypass) with their characteristics generated from a statistical analysis using historical storm data for the time period 1940 through 2008 (Toro et al. 2011). Each storm has unique pressure deficit, radius to maximum winds, translation speed, storm heading, and landfall location. Among the 159 storms, pressure deficit ranges from 13 to 90 hPa,

radius to maximum winds from 18 to 120 km, and translation speed from 2.1 to 11.3 m s⁻¹ (Fig. 2a). In the plot, the storm index is populated by abscissa values not storm number. According to the SSHS, 55 storms rank as Category 1 at landfall, 29 as Category 2, 52 as Category 3, 23 as Category 4, and 0 as Category 5. Storm heading varies from -74 to +87 deg (clockwise from true north) and landfall location varies from 88.84°W and 30.39°N as the western boundary to 83.52°W and 29.70°N as the eastern boundary covering

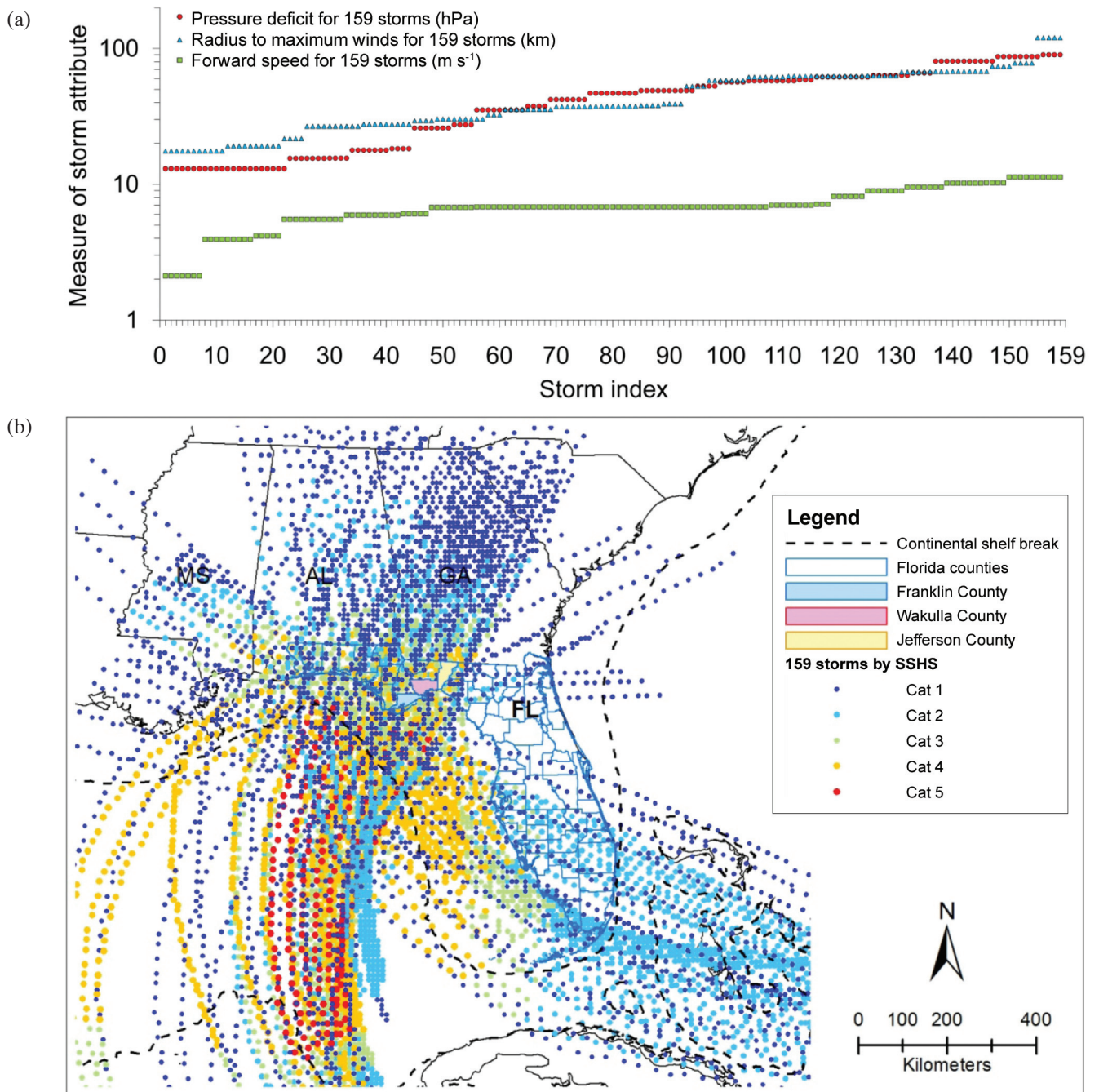


Fig. 2. (a) Attributes of 159 storms. Each categorical series is ranked in ascending order. (b) Storm tracks of 159 storms symbolized by Saffir-Simpson Hurricane Scale.

600 km of coastline (Fig. 2b). The set of 159 storms was comprehensive in covering a wide range of storm attributes. Note the only variability among the 159 storm surge simulations was with storm forcing in that all other model settings, initial conditions, boundary conditions, and model parameters, were held constant.

Two sets of production runs were performed using the 159 storms (Toro et al. 2011): ADCIRC + SWAN, hereafter referred to as SURGE + WAVES, and ADCIRC (without SWAN), hereafter referred to as SURGE ONLY. Each production run produced a MEO: 159 MEOWs for SURGE + WAVES and 159 MEOWs for SURGE ONLY. The frequency analysis utilized the MEOWs for the determination of 0.2% (= 1-in-500-year return-period) flooding surface (detailed later). The 500-year floodplain was the most extreme case considered in the frequency analysis and is used herein to represent extreme-case surge conditions (Toro et al. 2011). The flooding surface is a contour map of elevation values (m) that measure as: $H(x_n, y_n) = h_{\text{top}}(x_n, y_n) - h_{\text{bot}}(x_n, y_n)$, where h_{top} is the top elevation of the flooding surface relative to NAVD88 (North American Vertical Datum of 1988), h_{bot} is the bathymetric depth below NAVD88 ($-h$) or topographic elevation above NAVD88 ($+h$), and (x_n, y_n) signifies that the H and h values depend on discrete (subscript n) horizontal space (x and y). There are no negative H values (they would be illogical as defined above). H values equal to zero mean that the local space exists outside of the given return-period floodplain. Positive H values mean that the local space exists within the given return-period floodplain where the local height (or depth, depending on the perspective) of the flooding surface is equal to the numerical value of H .

4. STUDY OBJECTIVES

We define the floodplain with a polygon (area = 4955 km²) consisting of the ADCIRC mesh landward of the zero-elevation contour (Fig. 1e). The focus herein is on storm surge and wave-driven inundation within the floodplain as defined above.

The objectives of this study are: (i) to consolidate the storms that contribute to inundation extent (the extent of inundation into the floodplain), coverage (the overall surface area of the inundated floodplain) and the spatially variable 0.2% flooding surface down to a number less than the 159 storms used in the production runs; and (ii) to apply the methodology for the examination of dynamically based sea level rise impact on hurricane and tropical storm-induced flooding in Franklin, Wakulla, and Jefferson counties. The specific goals of this study are: (i) to assess and understand the characteristics of a set of synthetic storms used in a recent coastal flood mapping effort for Florida's Big Bend Region in the context of SSHS versus alternative classification; and (ii) to present an analysis of static versus dynamic response

due to sea level rise. The high resolution of the production run data combined with the comprehensiveness of the set of storms used in generating the data is exploited to meet the study objectives and to achieve the first goal. The results are interpreted in terms of storm attributes (pressure deficit, radius to maximum winds, translation speed, storm heading, and landfall location) and the physical processes during storms surge and waves. The methodology is applied to assess the dynamics of sea level rise impacts (detailed later) to address the second goal.

5. ASSESSMENT OF MAXIMUM ENVELOPES OF WATER (MEOWS)

Output included maximum envelopes of water (MEOWs), which are worst-case snapshots of flooding extent resulting from given storms, for Franklin, Wakulla, and Jefferson counties in Florida's Big Bend Region (see the National Hurricane Center 2011a for a definition). All MEOW outputs were assessed to produce maximums of the maximums (MOMs) (Fig. 3), which are worst-case snapshots of flooding extent resulting from "perfect" storm conditions (see the National Hurricane Center 2011b for a definition), one for SURGE + WAVES and one for SURGE ONLY. The inland boundaries of the MOMs represent the overall extent of inundation caused by all 159 storms. Each boundary was extracted as a continuous polyline: SURGE + WAVES length equaled 736 km; and SURGE ONLY length equaled 725 km. The areas covered by the MOMs within the defined floodplain were calculated: SURGE + WAVES equaled 1924 km²; and SURGE ONLY equaled 1858 km². The SURGE + WAVES boundary extends further inland than the SURGE ONLY boundary; however, such instances are localized and limited. In fact, this exposes only 66 km² of additional inundation area due to waves which is little over 1% of the entire floodplain.

The MOMs from SURGE + WAVES and SURGE ONLY were compared to one another on a node-by-node basis. For each mesh node, an absolute difference was calculated as $\Delta_{\text{abs}} = (\text{SURGE} + \text{WAVES}) - (\text{SURGE ONLY})$ along with a relative difference calculated as $\Delta_{\text{rel}} = 100\% \times \Delta_{\text{abs}} \div (h + \text{MOM}_{\text{SURGE ONLY}})$. Figure 4a shows a contour plot of absolute differences and Fig. 4b shows a contour plot of relative differences. For the most part, absolute differences range from 0 to 40 cm and relative differences range from 0% to 20%. The mean absolute difference is 18 cm and the standard deviation is ± 5 cm. The mean relative difference is 7% and the standard deviation is $\pm 4\%$. Wave influence reaches ≈ 15 km inland over the eastern half (≈ 60 km) of the domain. Note this location coincides with Apalachee Bay and Ochlocknee Bay. Clearly, the bays act to enhance waves regionally along the ≈ 60 -km length of coastline and behind Ochlocknee Bay. Furthermore, the sharp angle ($\approx 135^\circ$) in the coastline together with the broad shelf of Florida's

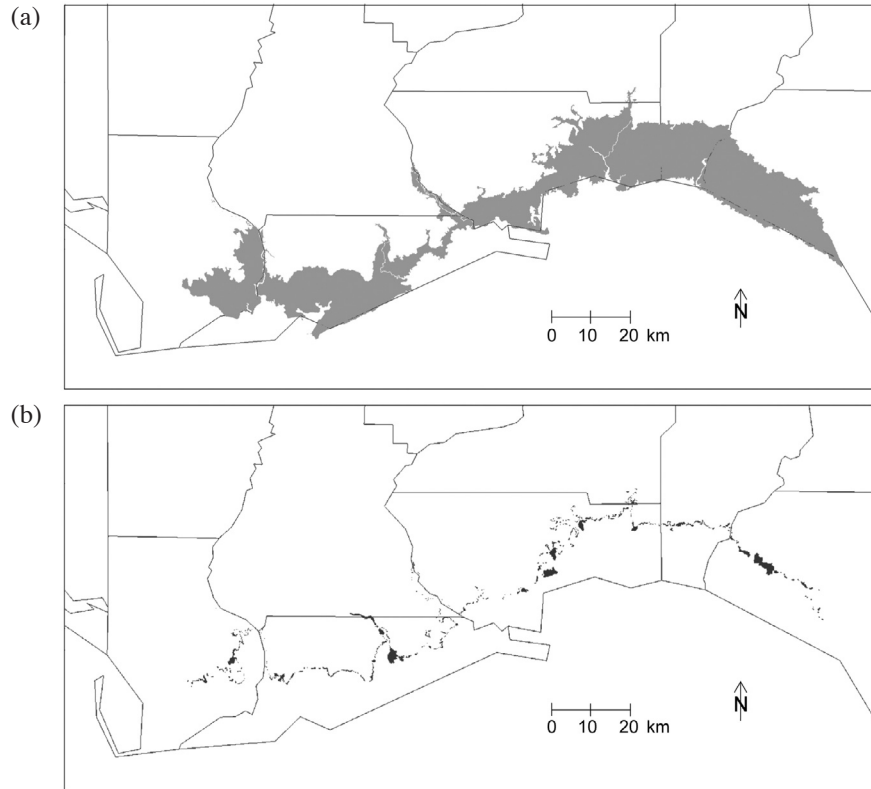


Fig. 3. (a) SURGE ONLY: maximum of maximums (MOM) (■) within a defined floodplain. (b) MOM (■) for SURGE + WAVES but not for SURGE ONLY.

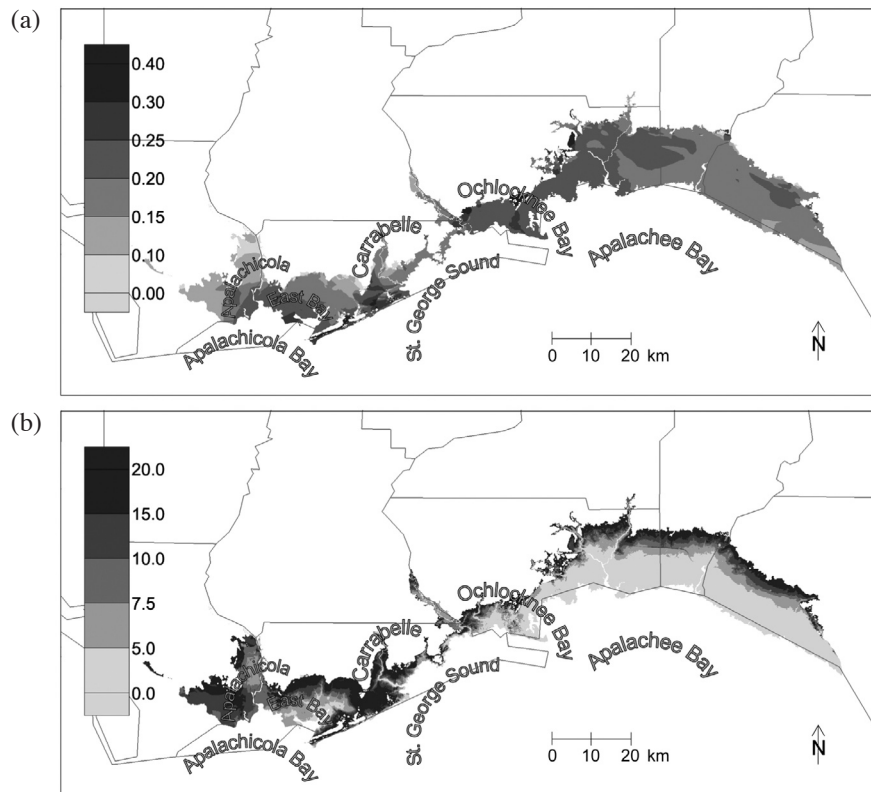


Fig. 4. Difference of maximums of maximums (MOMs) within a defined floodplain - SURGE + WAVES minus SURGE ONLY: (a) absolute (m); and (b) relative (%) to MOM (SURGE ONLY) plus bathymetric depth/topographic elevation.

west coast (Fig. 1c) acts to direct storm surge and waves northward into Apalachee and Ochlocknee Bays. Other areas where short waves are transferring momentum to the long-wave surge include: behind St. George Sound into the city of Carrabelle with an inland reach on the order of kilometers; and behind Apalachicola Bay into East Bay and the city of Apalachicola with an inland reach of 5 - 10 km. The barrier islands that stretch along the western ≈ 60 km of the domain (Fig. 1b) are not overtly protective with regard to waves riding on top of the storm surge and contribute to inland flooding. The relative influence of waves is moderate (greater than 7.5%) throughout Apalachicola and East Bays, large (greater than 15%) behind St. George Sound and into Carrabelle, and small (less than 5%) for most of the floodplain behind Ochlocknee and Apalachee Bays. There are very few instances where relative percentages are greater than 10%, most notably in the backs of Apalachicola and East Bays. Overall, wave influence was found to be low, for the most part on the order of only single percentage points, suggesting that wave contribution was minimal in Florida's Big Bend Region for the present floodplain analysis.

The MEOW outputs (the 159 corresponding to SURGE ONLY) were compared on a node-by-node basis to the MOM (SURGE ONLY). For each mesh node, the number of the MEOW output (correspondent to the storm number) with the MEOW value closest to the MOM value was determined and stored as an integer $j = 1, \dots, 159$. The percentage of nodal coverage of the MOM extent within the defined floodplain was calculated for each storm: $P_{\text{cMOM}, C} = 100\% \times N_{\text{cMOM}, C} \div N_{\text{cMOM}, T}$, where P is a percentage measure and N are count measures, the 'cMOM' subscript stands for 'coverage of MOM,' and the 'C' and 'T' subscripts stand for 'contributing' and 'total.' Figure 5a shows the full range of storms with an inset of the top 7 contributing storms: numbers = 85, 84, 83, 65, 64, 86, and 82. These 7 storms are identified as the top contributors (Table 3): (i) because each contributes to more than 1%; (ii) because they cumulatively contribute to greater than 90% (actually 92%). In fact, the top 2 contributing storms (numbers = 85 and 84) together contribute to a majority of the MOM (55%). These top 7 contributing storms have (Table 2) high pressure deficits (56 - 87 hPa), large radii to maximum winds (37 - 68 km), low-to-moderate translation speeds (4.2 - 6.8 m s⁻¹), and storm headings from (+28 to +61 deg, clockwise from north), and make landfall off-center, typically to the west of the region of interest (Fig. 1c).

6. ASSESSMENT OF 500-YEAR FLOODPLAIN

The 159 MEOW outputs were compared on a node-by-node basis to the 0.2% flooding surface (Fig. 6a). For each mesh node, the number of the MEOW output (corresponding to the storm number $j = 1, \dots, 159$) with the MEOW value closest to the flooding surface value was determined.

Figure 6b shows the spatial pattern of the top 5 contributing storm numbers (65, 83, 84, 64, and 66) for the 0.2% flooding surface (SURGE ONLY). Note the vast coverage of the flooding surface by just these top 5 contributing storms of the 159 original storms.

The percentage of nodal coverage of the entire inundation extent within the defined floodplain was calculated on the basis of each storm contributing to the return-period flooding surface: $P_{\text{cMOM}, \text{fs}, C} = 100\% \times N_{\text{cMOM}, \text{fs}, C} \div N_{\text{cMOM}, T}$, where P is a percentage measure and N are count measures, the 'cMOM' and 'fs' subscripts stand for 'coverage of MOM' and 'flooding surface,' and the 'C' and 'T' subscripts stand for 'contributing' and 'total.' Figure 5b shows the full range of storms highlighting the top 5 storms (numbers = 65, 83, 84, 64, and 66) contributing to the 0.2% flooding surface (SURGE ONLY). The flooding surface has only 14 contributing storms with the top 2 storms each contributing to greater than 20% of the flooding surface. This can be explained in terms of a frequency analysis whereby distributions for extreme cases (like 0.2% = 1-in-500-year return-period) are based on a limited set of extreme events. Table 4 reports the percent contributions P matching the nodal values of the 0.2% flooding surface for the 14 highest ranking (by numerical value of P) storms. Cumulative percent contributions ΣP are also tabulated which provides the coverage of flooding surface that is determined by a certain number of highest ranking storms. The 14 highest ranking storms accumulate to 100% P (full coverage). The top 5 storms yield 76% of the flooding surface and the top 10 storms 91%.

7. SEA LEVEL RISE APPLICATION

Zervas (2001) reported values of sea level rise for the tidal gaging stations maintained by the National Oceanic and Atmospheric Administration (NOAA) based on a linear regression analysis. Furthermore, sea level rise has been shown to consist of a linear term plus an accelerative term (International Panel on Climate Change 2007): $\text{SLR}(t) = 1.7t + bt^2$, where SLR is sea level rise in mm, t is time in yr, 1.7 is the linear rate in mm yr⁻¹, and b is the accelerative rate in mm yr⁻². Using linear and second-order regression analysis, Walton (2007) reported values of sea level rise for five NOAA tidal gaging stations located in Florida. Sea level rise for 2006 - 2080 was forecast at 0.13 m for linear increase and 0.34 m for second-order increase. For the following sea level rise application, we apply 15.2 cm (6 in) and 30.5 cm (1 ft).

The top 5 storms (numbers 65, 83, 84, 64, and 66) contributing to the 0.2% flooding surface were each rerun for baseline and sea level rise (+30.5 cm and +15.2 cm) conditions with ADCIRC. The simulations were performed exactly the same as how the production runs were performed (Toro et al. 2011) except that sea level rise (+30.5 cm and

+15.2 cm) was either incorporated into the model (sea level rise) or not (baseline). A MEOW was produced from each of the model runs. The MEOW outputs were assessed for extent of inundation to produce a set of MOMs. Those are the results from the dynamic approach. For the static ap-

proach, the baseline MOM was elevated domain-wide by sea level rise of 15.2 cm (6 in) and 30.5 cm (1 ft) allowing additional inland regions to become inundated based on the topography in relation to the elevated MOM (cf. Zhang 2011). The procedures above (dynamic and static

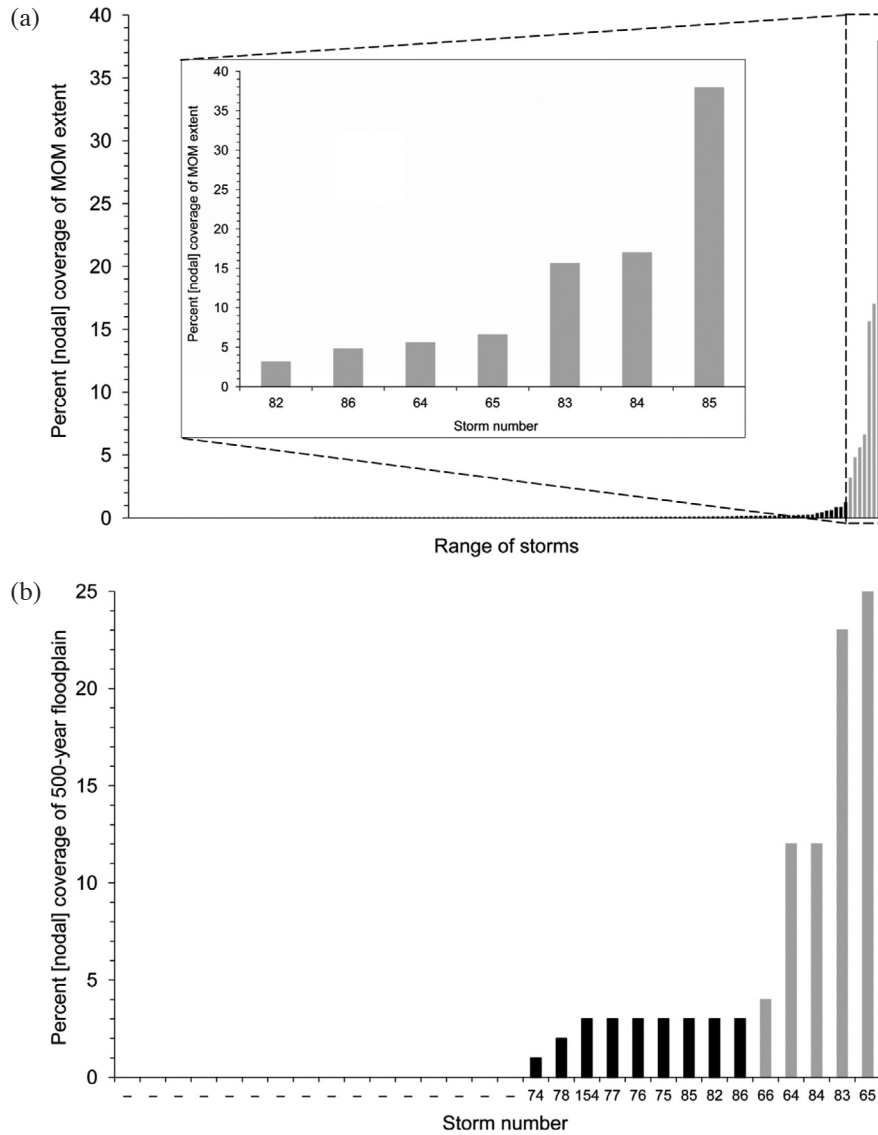


Fig. 5. SURGE ONLY. (a) Storm numbers matching nodal values of maximum of maximums. Top 7 contributing storms (■). x-axis for background panel not labeled to avoid clutter. (b) Storm numbers matching nodal values of 0.2% (1-in-500-year return-period) flooding surface. Top 5 contributing storms (■).

Table 3. Percent contributions P (%) matching nodal values of maximum envelope of water of SURGE ONLY for 7 highest ranking (by numerical value of P) storms (#). ΣP = cumulative percent contribution (%).

Rank	#	P	ΣP	Rank	#	P	ΣP
1	85	38	38	5	64	6	84
2	84	17	55	6	86	5	89
3	83	16	71	7	82	3	92
4	65	7	78				

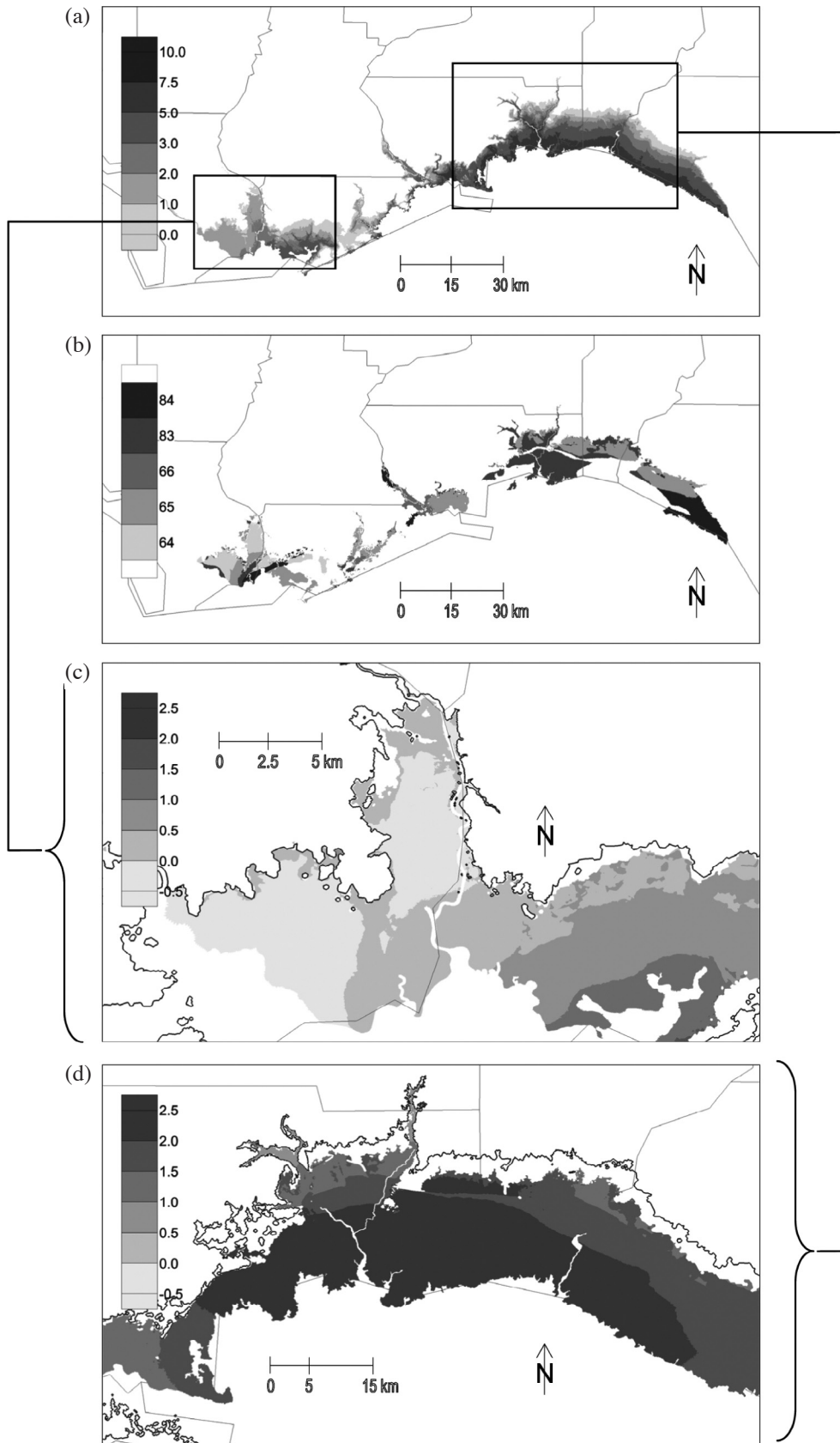


Fig. 6. SURGE ONLY within a defined floodplain: (a) 0.2% (1-in-500-year return-period) flooding surface (m); and (b) storm numbers (integers $-j = 65, 83, 84, 64,$ and 66) (top 5) contributing to 0.2% (= 1-in-500-year return-period) flooding surface. (c) (d) Absolute difference of (SURGE ONLY) maximum of maximums (MOM) minus 0.2% (1-in-500-year return-period) flooding surface (m) within a defined floodplain. MOM boundary (—).

Table 4. Percent contributions P (%) matching nodal values of 0.2% (1-in-500-year return-period) flooding surface for 14 highest ranking (by numerical value of P) storms (#). ΣP = cumulative percent contribution (%).

Rank	#	P	ΣP	Rank	#	P	ΣP
1	65	25	25	8	85	3	85
2	83	23	48	9	75	3	88
3	84	12	60	10	76	3	91
4	64	12	72	11	77	3	94
5	66	4	76	12	154	3	97
6	86	3	79	13	78	2	99
7	82	3	82	14	74	1	100 ^a

^a 100% indicates complete coverage of a floodplain.

approaches) were applied also for the case of astronomic tides only (no storm forcing). For this, the model was applied in astronomic tide-only mode (no storm forcing) for baseline and sea level rise (+30.5 and +15.2 cm) conditions. For reference, details on implementation of the model, including performance of baseline conditions, are contained in Atkinson et al. (2011).

Figures 7 and 8 show the baseline MOM versus sea level rise MOMs (+30.5 and +15.2 cm, respectively) for dynamic and static assessment of storm surge associated with the top 5 storms contributing to the 0.2% flooding surface (numbers 65, 83, 84, 64, and 66). For the dynamic approach, sea level rise of +30.5 cm (+1 ft) impacts 52 km² (20 mi²) of the defined floodplain with sea level rise of +15.2 cm (+6 in) impacting 28 km² (11 mi²) of the area. For the static approach, sea level rise of +30.5 cm (+1 ft) impacts 50 km² (19 mi²) of the defined floodplain with sea level rise of +15.2 cm (+6 in) impacting 30 km² (11 mi²) of the area. By this comparison, the static approach yields approximately the same area of sea level rise impact as does the dynamic approach; however, the sea level rise impact differs between the two; refer to the dotted ovals in Figs. 7 and 8, which indicate notable regions of dynamic sea level rise impact. The static approach essentially adds a band of sea level rise impact along the entire baseline extent whereas the dynamic approach is deterministically establishing where the sea level impact will occur.

Figures 9 and 10 show the baseline MOM versus sea level rise MOMs (+30.5 and +15.2 cm, respectively) for dynamic and static assessment of astronomic tides only (no storm forcing). For the dynamic approach, sea level rise of +30.5 cm (+1 ft) impacts 87 km² (34 mi²) of the defined floodplain with sea level rise of +15.2 cm (+6 in) impacting 27 km² (10 mi²) of the area. For the static approach, sea level rise of +30.5 cm (+1 ft) impacts 63 km² (24 mi²) of the defined floodplain with sea level rise of +15.2 cm (+6 in) impacting 23 km² (9 mi²) of the area. By this comparison, the static approach underestimates the area of sea level rise impact relative to the dynamic approach by a ratio as low as

≈2:3, more so for applied sea level rise of +30.5 cm (+1 ft) than for applied sea level rise of +15.2 cm (+6 in). The dotted ovals in Figs. 9 and 10 indicate notable regions of dynamic sea level rise impact.

Figure 11 shows contour plots of absolute differences (on a node-by-node basis) between the sea level rise MOMs (+30.5 and +15.2 cm) and the baseline MOM for the dynamic assessment of storm surge from the top 5 contributing storms (numbers 65, 83, 84, 64, and 66). Contour difference plots are not shown for the static assessment since it is a uniform surface the value of the applied sea level rise. The scales on the contour plots are set up to emphasize where dynamic differences are 0.305 ± 0.076 m (1 ft \pm 3 in) and 0.153 ± 0.076 m (6 in \pm 3 in), which populate much of the defined floodplain for sea level rise of +30.5 cm (+1 ft) and sea level rise of +15.2 cm (+6 in), respectively. There are, however, localities where dynamic differences reach beyond ± 0.076 m (± 3 in) of the applied sea level rise. This is more the case for a sea level rise of +30.5 cm (+1 ft) than for a sea level rise of +15.2 cm (+6 in). As an additional observation, note how the dynamic differences near the inland extent tend to be less than the dynamic differences within the open interior. Figure 12 shows contour plots of absolute differences (on a node-by-node basis) between the sea level rise MOMs (+30.5 and +15.2 cm) and the baseline MOM for the dynamic assessment of astronomic tides only (no storm forcing) which shows a fairly uniform surface the value of the applied sea level rise; though, there are a few limited localities where dynamic differences reach beyond ± 0.076 m (± 3 in) of the applied sea level rise with this being more the case for a sea level rise of +30.5 cm (+1 ft) than for a sea level rise of +15.2 cm (+6 in).

8. RECAP AND DISCUSSION

Production runs using ADCIRC for circulation modeling and SWAN for wave modeling provided 159 MEOW outputs based on 159 synthetic storms; tropical storms and hurricanes making landfall and bypassing landfall to analyze

Franklin, Wakulla, and Jefferson counties in Florida's Big Bend Region (Toro et al. 2011). Contour plots of maximum envelopes of water (MEOWs) were examined for inundation extent and coverage and compared to the 0.2% flooding surface.

Storm numbers 85, 84, 83, 65, 64, 86, and 82 are identified (Table 3) as the top 7 storms contributing to the maximum of maximums (MOM) where (i) each storm contributes greater than 1% of the MOM and (ii) the storms cumulatively contribute greater than 90% (actually 92%) of the MOM. The attributes of these storms range thus: pressure deficit = 59 - 87 hPa, radius to maximum winds = 37 - 68 km, translation speed = 4.2 - 6.8 m s⁻¹, and storm heading from +23 to +61 deg, clockwise from north (Table 2). In relation to the full set of 159 storms, these storms have high pressure deficits, large radii to maximum winds, and low-to-moderate translation speeds (Fig. 13a). These storms

have northeastern headings and make landfall off-center, typically to the west of the region of interest (Fig. 13b).

The top 7 storms contributing to the MOM cumulatively account for 81% of the 0.2% flooding surface (Table 4). However, on a singular basis, each storm accounts for no more than 25% of the flooding surface. This is particularly relevant in that a region cannot and should not define any particular storm as being the sole contributor to the statistical flooding surface. For instance, historical hurricanes (see Table 2 for select examples) are often associated with a return period when in fact, a region should define return periods for particular storm attributes as they contribute to inundation hazards within the given region. Further, this should be done on a spatially dependent basis, be it discrete as is the case here or continuous as shown in Irish et al. (2009) and Resio et al. (2009). On the other hand, the top 5 storms (numbers 65, 83, 84, 64, and 66) contributing to the

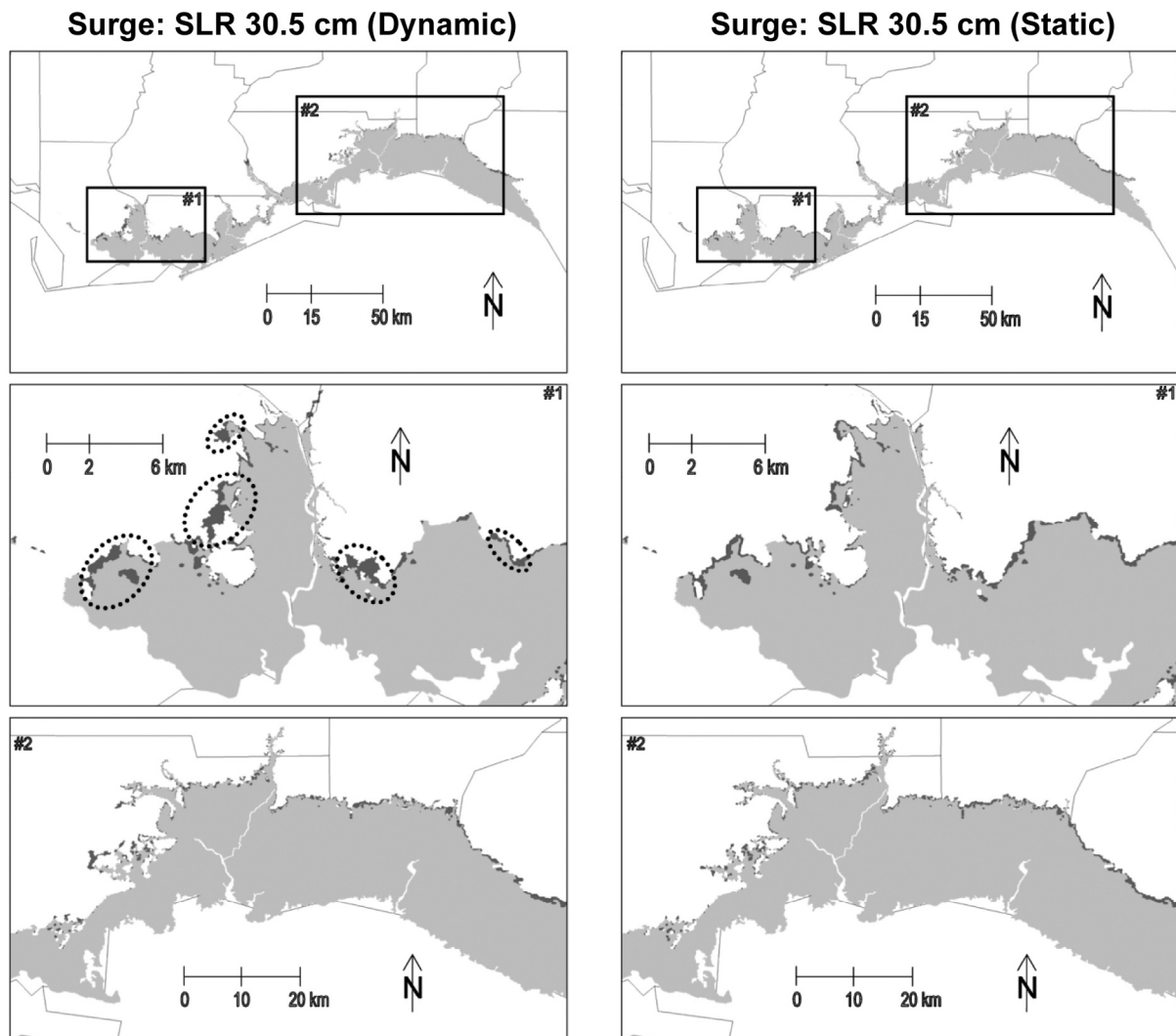


Fig. 7. Baseline (■) and sea level rise (+30.5 cm, dynamic and static) (■ + ■) maximums of maximums within a defined floodplain for storm surge from the top 5 contributing storms (numbers 65, 83, 84, 64, and 66). Dotted ovals indicate notable regions of dynamic sea level rise (+30.5 cm) impact (■).

0.2% flooding surface yield 76% (coverage) of the flooding surface. This means just 5 storms can be used to provide over three-quarters coverage of the flooding surface.

Another outcome from applying this approach is the result showing that the top 2 contributing storms (numbers 85 and 84) together contribute to 55% of the MOM (Fig. 5a) but contribute only 15% of the 0.2% flooding surface (Fig. 5b). To examine this further, the differences in extent (horizontal coverage, viz. inland reach) and height (vertical) between the MOM and the 500-year floodplain were determined. Figures 6c and 6d show these differences for western and eastern general localities (the two insets) within the defined floodplain. Note the greater horizontal extent of the MOM relative to the 500-year floodplain (additional area calculated as 195 km²) as well as the mostly positive vertical differences between the two (ranging between -0.5 and +2.5 m). Note also the greater differences

(both horizontal and vertical) for the eastern inset than for the western inset indicating that the greatest surge (MOM), i.e., greater than extreme surge (500-year floodplain), occurs on the eastern half of the domain where the coastal geometry of Florida’s Big Bend Region forms a natural cusp that facilitates the growth of storm surge (as opposed to the western half of the domain which has less of these kinds of surge-amplification effects). Storms 85 and 84 were strong storms that had track histories and landfall locations (Fig. 13b) which allowed them to be the greatest surge generators of all 159 storms assessed, and hence they contributed greatly to the MOM. Recall the MOM representing the worst-case snapshot of flooding extent resulting from “perfect” storm conditions (see the National Hurricane Center 2011b for a definition). On that basis, the strongest storms with near-“perfect” approach and strike location (storms 85 and 84) contribute most to the MOM. Storms 65 and

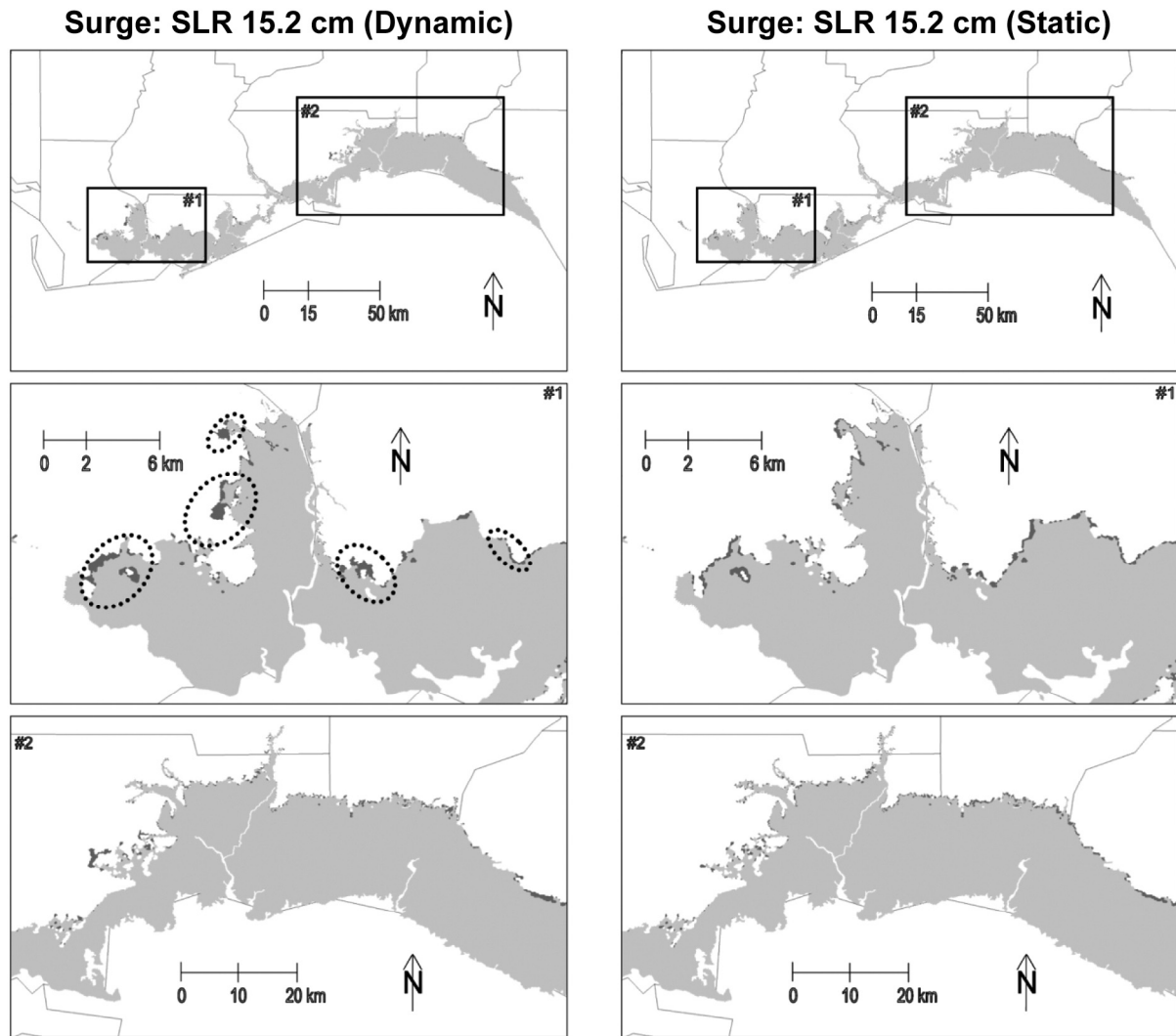


Fig. 8. Baseline (■) and sea level rise (+15.2 cm, dynamic and static) (■ + ■) maximums of maximums within a defined floodplain for storm surge from the top 5 contributing storms (numbers 65, 83, 84, 64, and 66). Dotted ovals indicate notable regions of dynamic sea level rise (+15.2 cm) impact (■).

64 were also strong storms, though not as strong as storms 85 and 84, and struck the coast more obliquely than storms 85 and 84, which were more direct in their hits (Fig. 13b); however, they were still extreme surge generators, in fact, together they contributed 37% of the 0.2% flooding surface. Recall the 500-year floodplain being the most extreme case extracted in the frequency analysis (Toro et al. 2011) and considered herein to represent extreme-case surge conditions. On that basis, those stronger-than-average storms, not the strongest of the 159 storms possible, with less-than-“perfect” approach and strike location (storms 65 and 64) contribute most to the 500-year floodplain.

Note the categorization of the top 7 storms, i.e., those contributing to the MOM (Table 2): none of them are SSHS Category 5; five of them are SSHS Category 4; and two of them are SSHS Category 3. The HII and HHI values are estimated using Eqs. (1) and (2) with reference values $V_{max,0}$

equal 33 m s^{-1} (equivalent to Cat 1 on SSHS), $R_{max,0}$ equal 54 km (30 mi), and S_0 equal 6.7 m s^{-1} (15 mph). The HII values reflect the SSHS categorization since both are primarily based on hurricane intensity. The HHI values, however, suggest that the additional influencing factors, i.e., radius to maximum winds and translational speed, contribute to storm surge-induced inundation. In fact, the HHI value = 13.3 for storm numbers 65 and 64 is comparable to the HHI values = 11.9 and 14.6 for Hurricanes Andrew and Katrina. Further, storm track and landfall location (Fig. 13b) are of paramount influence with respect to storm surge generation and the associated coastal flooding (Fig. 5).

As an engineering implication, identifying the top-contributing storms can permit for more efficient inundation modeling and analysis in that simulating with just the top-contributing storms generates much of the same response as when simulating with the entire set of 159 storms. For

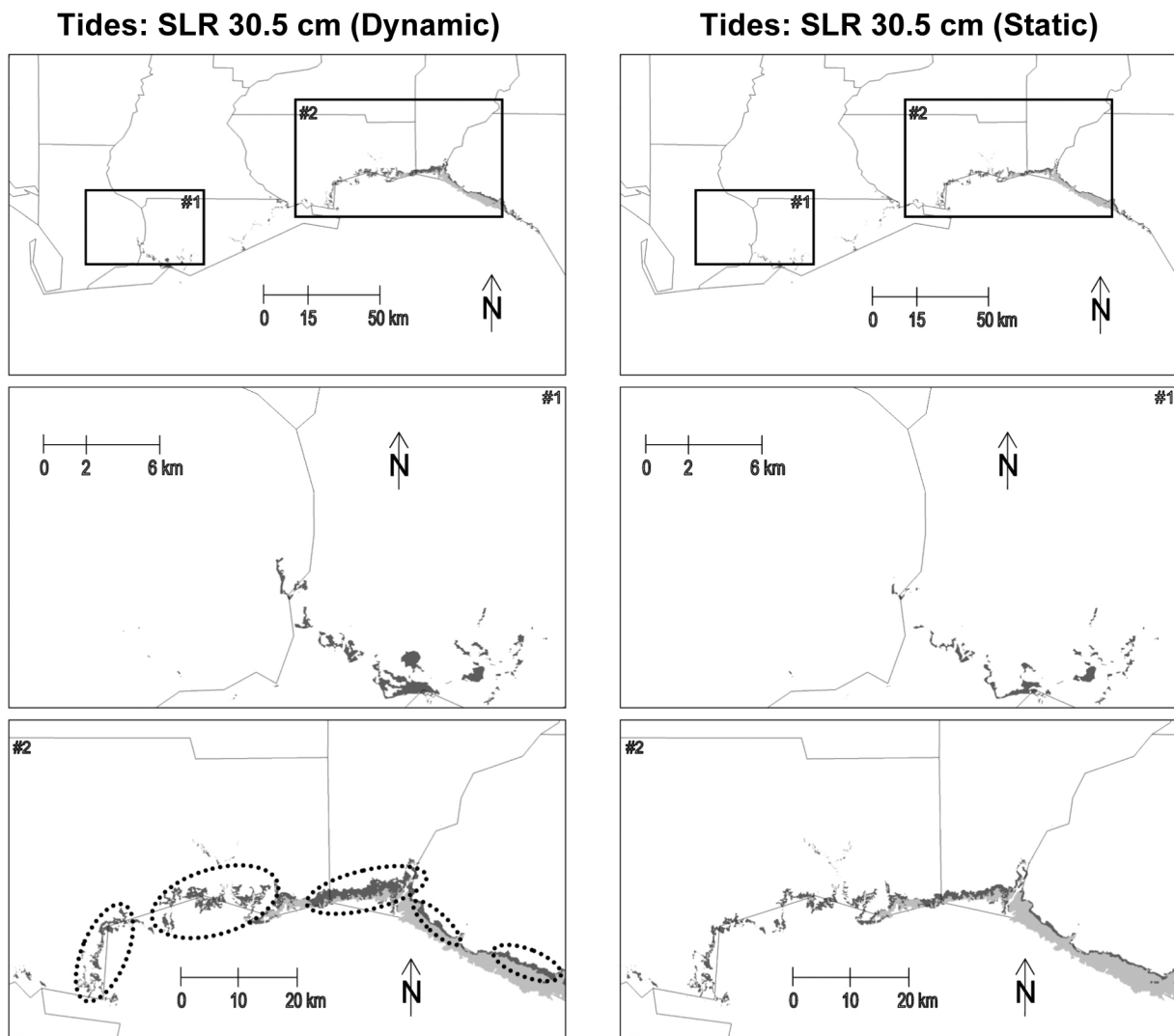


Fig. 9. Baseline (■) and sea level rise (+30.5 cm, dynamic and static) (■ + ■) maximums of maximums within a defined floodplain for astronomic tides only (no storm forcing). Dotted ovals indicate notable regions of dynamic sea level rise (+30.5 cm) impact (■).

instance, the cost savings of running only the top 5 storms contributing to the 0.2% flooding surface versus running all 159 storms is almost 97%. The benefit is that 76% coverage of the flooding surface is captured by running only 5 storms. Note that approximately one hour of computer time is required to run a 5-day storm surge simulation (ADCIRC) with 855445 mesh nodes and a 1.0 second time step, when parallelized over 256 cores. The methodology presented in this paper demonstrates its applicability to Florida’s Big Bend Region; however, it would be easily transferrable to other regions.

There is societal relevance to this work. Economic activity along the United States’ coasts continues to increase (Rappaport and Sachs 2003). Along with this comes increased development and residence in the coastal floodplain which means that a continually increasing amount of the population will be at high risk of coastal flooding. Modeled

forecasts also indicate increased threats of sea level rise and the associated impact on coastal flooding (Parker 1991). At the same time, to guide future development and residence in the coastal floodplain, the United States establishes Flood Insurance Rate Maps (FIRMs). It is in this context that the methodology presented in this paper (i) uses as input results from a highly defensible and cooperative re-evaluation study of the FIRMs for Franklin, Wakulla, and Jefferson counties in Florida’s Big Bend Region (Gangai et al. 2011) and (ii) generates as output a set of storms (far reduced from the full set of 159) that contribute to frequency-based (0.2% flooding surface) coastal flooding in Franklin, Wakulla, and Jefferson counties in Florida’s Big Bend Region. The output supplies information on what types of storms (attributes) lead to the various patterns of inundation (where flooding will occur) and can be readily interpreted by the public.

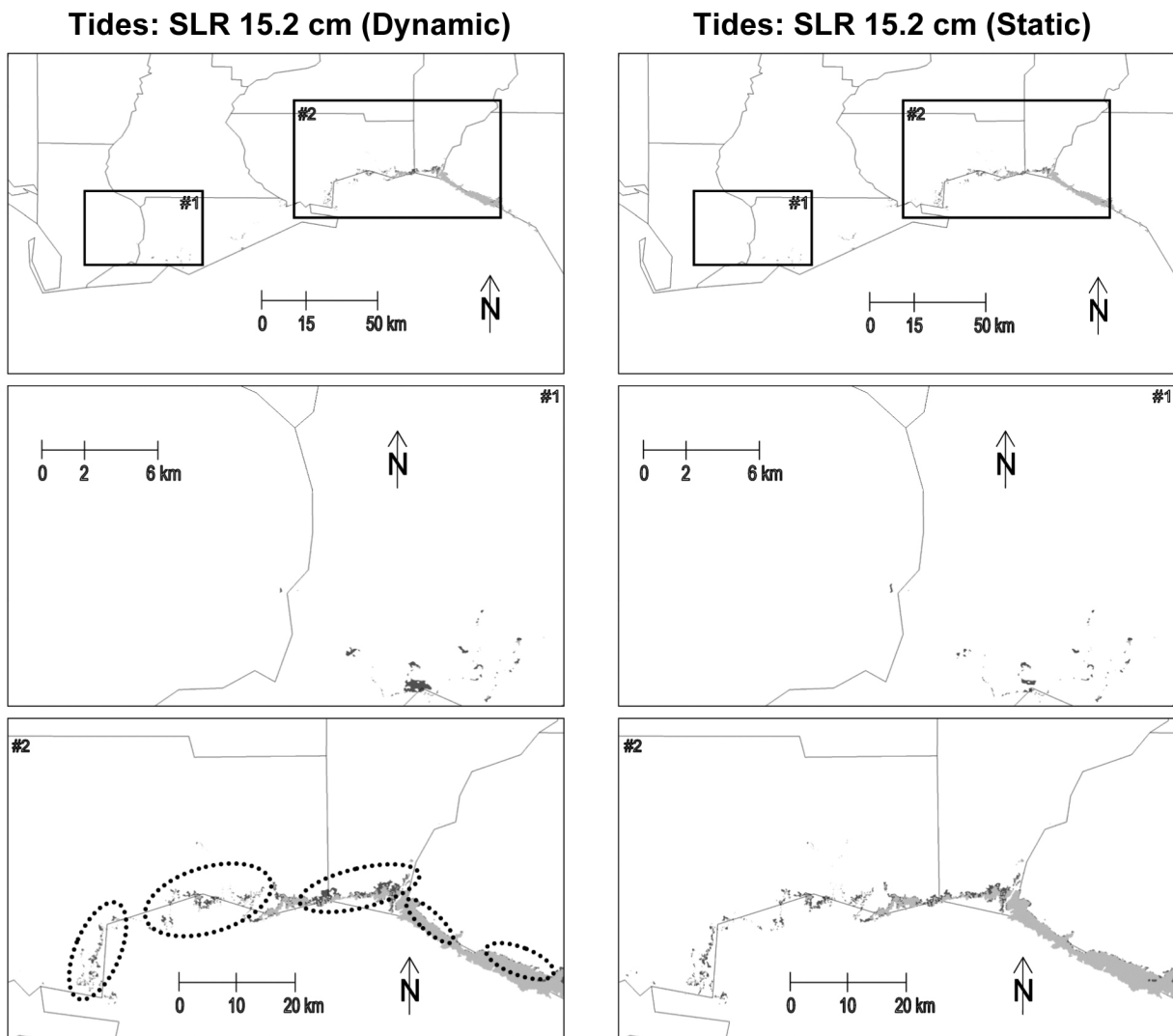


Fig. 10. Baseline (■) and sea level rise (+15.2 cm, dynamic and static) (■ + ■) maximums of maximums within a defined floodplain for astro-nomic tides only (no storm forcing). Dotted ovals indicate notable regions of dynamic sea level rise (+15.2 cm) impact (■).

Additionally, the output is also useful in guiding ongoing studies, e.g., dealing with sea level rise impact. In fact, this is demonstrated herein with an impact assessment (dynamic versus static) resulting in a 15.2 cm (6 in) and 30.5 cm (1 ft) of sea level rise. The dynamic results are reflective of the dynamics occurring in the face of sea level rise while the static results are an approximation of flooding caused by the elevated baseline conditions (MOM) in relation to the topography (Zhang 2011). Using a static approach to assess sea level rise impact, in the case of extreme storm surge for Florida's Big Bend Region, will generate approximately the same amount of impacted floodplain area relative to that dynamically predicted (Table 5), viz. the dynamic approach applied herein; however, the distribution of the sea level rise impact will differ between the two approaches (static versus dynamic) (Figs. 7 and 8). For astronomical tides only (no storm forcing), using a static approach

will underestimate the amount of impacted floodplain area relative to a dynamic approach (Figs. 9 and 10) herein shown to underestimate by a ratio as low as $\approx 2:3$ (Table 5). Alternatively, a dynamic approach will estimate as much as 1.5 times the amount of impacted floodplain area than will a static approach. A dynamic approach is preferred to a static approach on the basis that a dynamic approach dynamically projects sea level rise impact by deterministically establishing where sea level rise impact will occur. A dynamic approach, as opposed to a static approach, takes into account the dynamics of the processes interacting with sea level rise and the associated geometry (topography).

9. CONCLUSIONS

A methodology was applied to identify the storm characteristics (a subset of synthetic storms) that contribute to

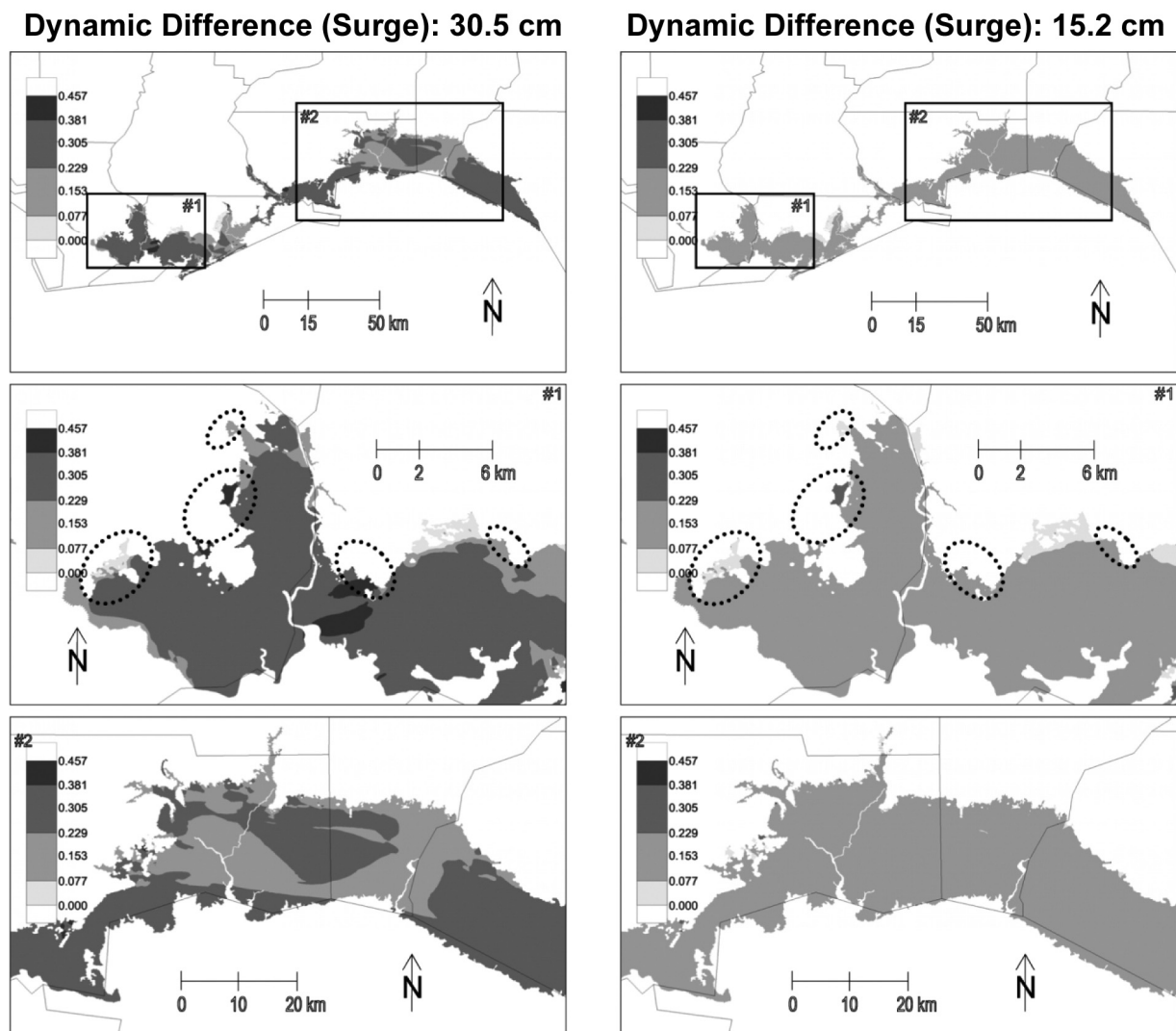


Fig. 11. Dynamic difference of maximums of maximums (MOMs) (m) - sea level rise MOMs (+30.5 and +15.2 cm) minus baseline MOM - within a defined floodplain for storm surge from top 5 contributing storms (numbers 65, 83, 84, 64, and 66).

hurricane and tropical storm-induced flooding, including the 500-year floodplain, in Florida's Big Bend Region. Of the identified subset of synthetic storms, they share the common characteristics of being strong (high pressure deficit), large (large radius to maximum winds), and slow-moving (low-to-moderate translation speed) hurricanes with headings in the northeast quadrant of the compass and landfalls west of the local area. The methodology, by generating a consolidated envelope of results, i.e., in identifying the top-contributing storms, expands on the capability of existing and new hurricane scales.

Of the physical processes associated with hurricane and tropical storm-induced flooding in Florida's Big Bend Region, storm surge is the primary driver. Waves were found not to add much further contribution to the overall water level (for the most part less than 10% and generally on the order of single percentage points). This is because Florida's

broad west shelf forces waves to break far offshore so that wave contribution is minimal at the coast and inshore. Conversely, the broad shelf (100 - 200 km) of Florida's west coast promotes the development of storm surge off the coast while the open bays along the coast funnel storm surge into the rivers and estuaries. These storm surge characteristics were shown to hold especially true for Florida's Big Bend Region because of the physical geography of the sharply angled ($\approx 135^\circ$) coastline, basin geology, and wide continental shelf. The coastal geometry of Florida's Big Bend Region forms a natural cusp that facilitates an increase in storm surge.

The dynamic and static impact assessment of sea level rise of 15.2 cm (6 in) and 30.5 cm (1 ft) in this study utilized the subset of synthetic storms. The dynamic assessment determined that, in the case of extreme storm surge, i.e., simulating with the identified top-contributing synthetic storms,

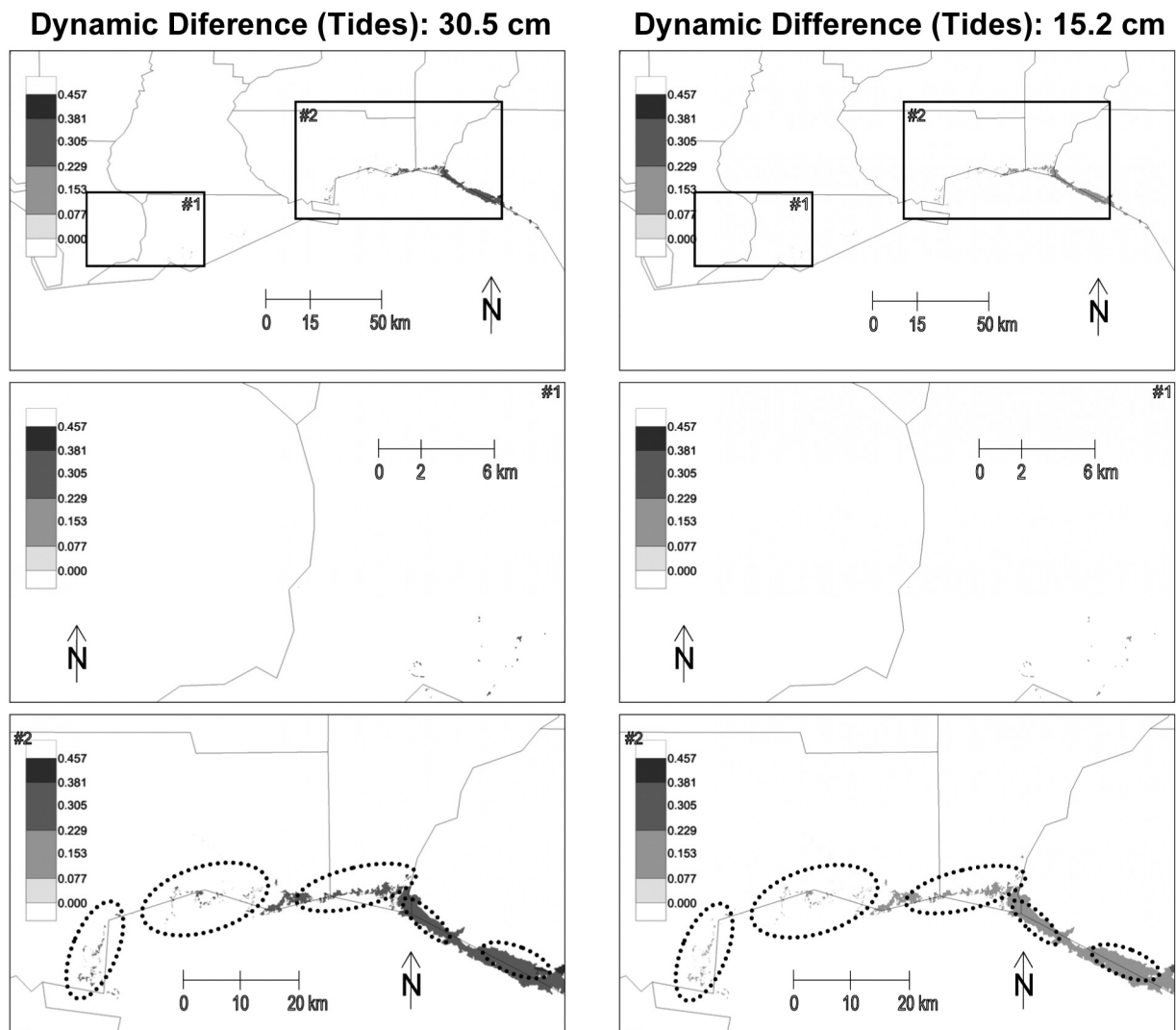


Fig. 12. Dynamic difference of maximums of maximums (MOMs) (m) - sea level rise MOMs (+30.5 and +15.2 cm) minus baseline MOM - within a defined floodplain for astronomic tides only (no storm forcing).

≈30 km² (≈10 mi²) of additional floodplain will become inundated by a sea level rise of 15.2 cm (6 in) with ≈50 km² (≈20 mi²) of additional floodplain becoming inundated by a sea level rise of 30.5 cm (1 ft). The static assessment produced approximately the same amount of additional inun-

dated floodplain as did the dynamic assessment; however, where the impact on sea level rise occurred differed between the two approaches (static versus dynamic). In the case of astronomic tides only (no storm forcing), using the static approach underestimated the amount of impacted floodplain

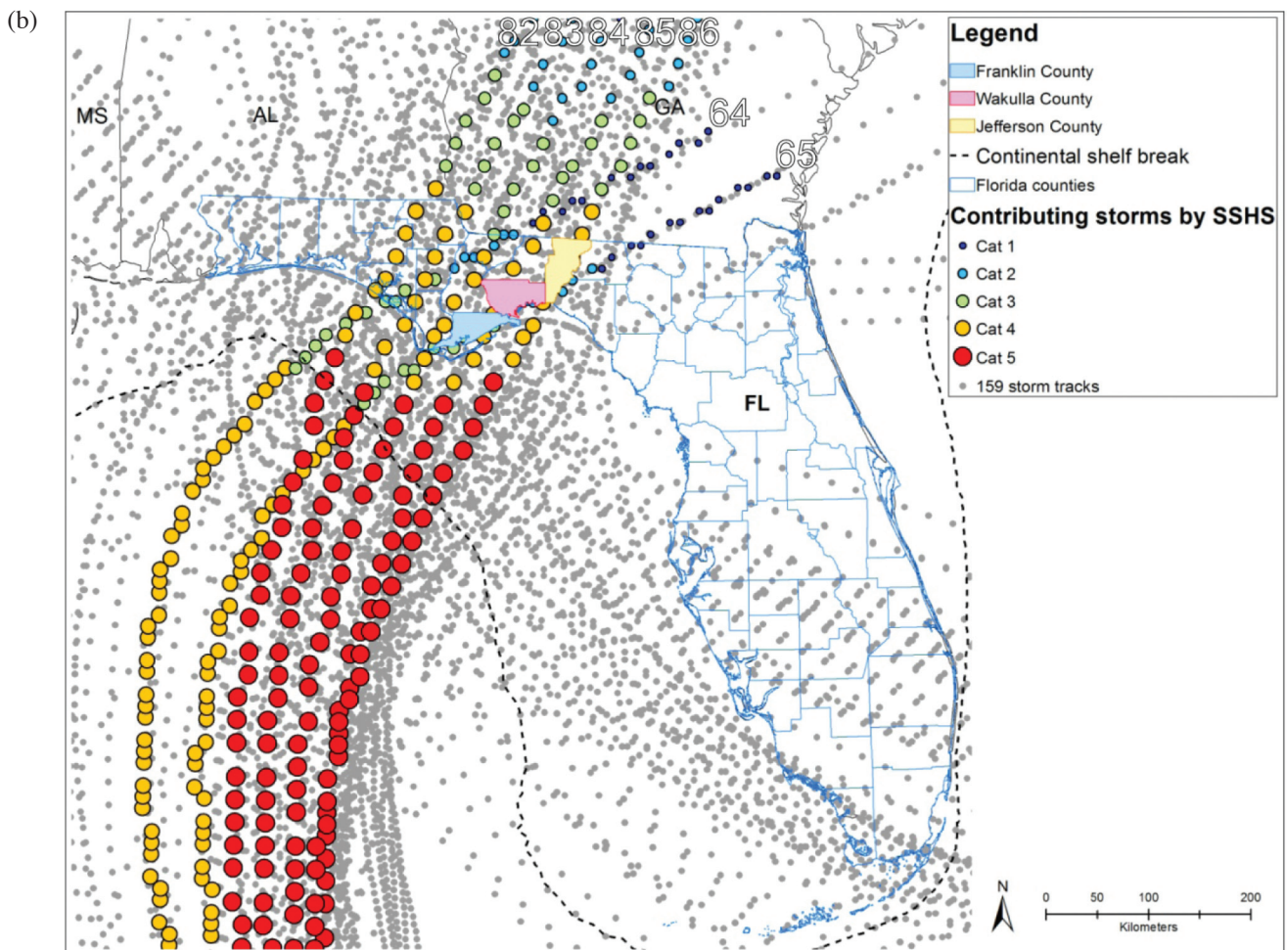
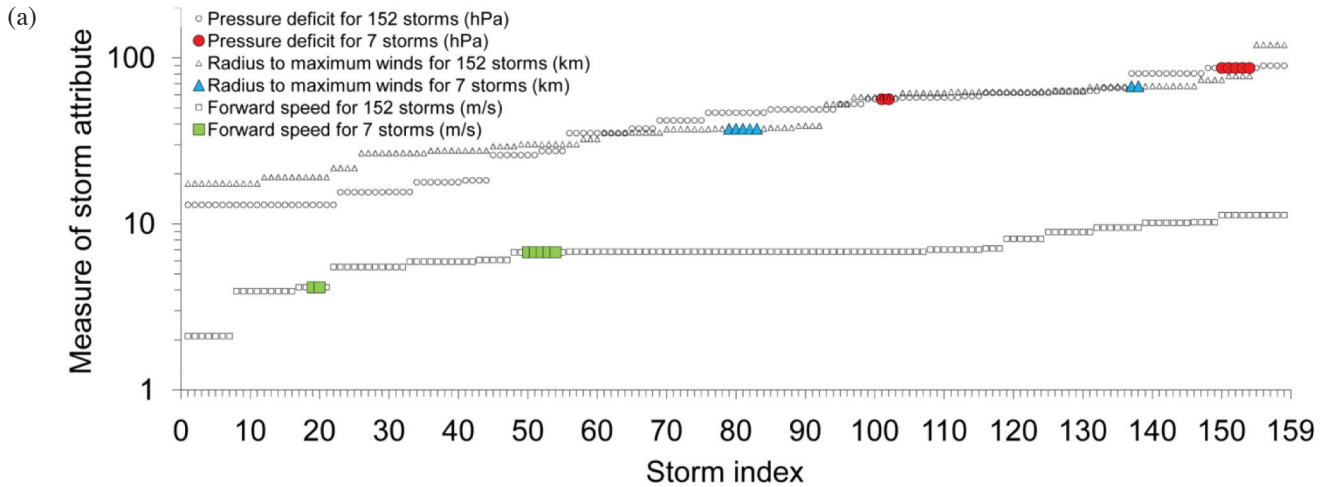


Fig. 13. (a) Attributes of 159 storms, 7 contributing storms and 152 other storms. Each categorical series is ranked in ascending order. (b) Storm tracks of 159 storms with top 7 contributing storms symbolized by Saffir-Simpson Hurricane Scale.

Table 5. The floodplain area affected by sea level rise.

Process	Sea level rise (m)	Approach	Area (km ²)
Storm surge	0.305	Dynamic	52
		Static	50
	0.152	Dynamic	28
		Static	30
Astronomic tides	0.305	Dynamic	87
		Static	63
	0.152	Dynamic	27
		Static	23

area relative to the dynamic approach by a ratio as low as $\approx 2:3$; alternatively, the dynamic approach led to as much as 1.5 times the amount of impacted floodplain area than that estimated by the static approach. In the case of both extreme storm surge and astronomic tides for Florida's Big Bend Region, sea level rise impact should be assessed as a dynamic process and not as a static process. Taking a static approach could miss dynamic interactions and it is advised that a dynamic approach be used to ensure their capture.

Acknowledgements This research was funded in part under Contract No. 07-1390 from Northwest Florida Water Management District (NFWFMD) and the Federal Emergency Management Agency (FEMA) and under Award No. NA10NOS4780146 from the National Oceanic and Atmospheric Administration (NOAA). The statements and conclusions are those of the authors and do not necessarily reflect the views of NFWFMD, FEMA, NOAA, or their affiliates. The authors thank Jeff Gangai for supplying the 500-year floodplain, John Atkinson and Hugh Roberts for their contribution to the original model simulations, Don Slinn for generating the wave fields, and Ammarin Daranpob for his valuable input and generation of graphics.

REFERENCES

- Atkinson, J., H. Roberts, S. C. Hagen, S. Zou, P. Bacopoulos, S. Medeiros, J. Weishampel, and Z. Cobell, 2011: Deriving frictional parameters and performing historical validation for an ADCIRC storm surge model of the Florida Gulf Coast. *Fla. Watershed J.*, **4**, 22-27.
- Blake, E. S., E. N. Rappaport, and C. W. Landsea, 2007: The deadliest, costliest, and most intense United States tropical cyclones from 1851 to 2006 (and other frequently requested hurricane facts). NOAA Technical Memorandum NWS TPC-5, Miami, Florida, 43 pp.
- Blake, E. S., E. N. Rappaport, and C. W. Landsea, 2011: The deadliest, costliest, and most intense United States tropical cyclones from 1851 to 2010 (and other frequently requested hurricane facts). NOAA Technical Memorandum NWS TPC-6, Miami, Florida, 49 pp.
- Emanuel, K., 2005: Increasing destructiveness of tropical cyclones over the past 30 years. *Nature*, **436**, 686-688, doi: 10.1038/nature03906. [Link]
- Gangai, J., S. C. Hagen, and R. Bartel, 2011: An overview of a FEMA coastal inundation study for the Big Bend Region of Florida. *Fla. Watershed J.*, **4**, 1-4.
- Hagen, S. C., A. K. Zundel, and S. Kojima, 2006: Automatic, unstructured mesh generation for tidal calculations in a large domain. *Int. J. Comput. Fluid Dyn.*, **20**, 593-608, doi: 10.1080/10618560601046846. [Link]
- International Panel on Climate Change, 2007: Climate change 2007: The physical science basis. In: Solomon, S., D. Qin, M. Manning, Z. Chen, M. Marquis, K. B. Averyt, M. Tignor, and H. L. Miller (Eds.), Contribution of Working Group I to the Fourth Assessment Report on the Intergovernmental Panel on Climate Change, Summary for Policymakers, Cambridge University Press, Cambridge, United Kingdom, 996 pp.
- Irish, J. L. and D. T. Resio, 2010: A hydrodynamics-based surge scale for hurricanes. *Ocean Eng.*, **37**, 69-81, doi: 10.1016/j.oceaneng.2009.07.012. [Link]
- Irish, J. L., D. T. Resio, and J. J. Ratcliff, 2008: The influence of storm size on hurricane surge. *J. Phys. Oceanogr.*, **38**, 2003-2013, doi: 10.1175/2008JPO3727.1. [Link]
- Irish, J. L., D. T. Resio, and M. A. Cialone, 2009: A surge response function approach to coastal hazard assessment. Part 2: Quantification of spatial attributes of response functions. *Nat. Hazards*, **51**, 183-205, doi: 10.1007/s11069-009-9381-4. [Link]
- Kantha, L., 2006: Time to replace the Saffir-Simpson hurricane scale? *Eos, Trans., AGU*, **87**, 3, doi: 10.1029/2006EO010003. [Link]
- Kantha, L., 2008: Comments: Tropical cyclone destructive potential by integrated kinetic energy. *Bull. Am. Meteorol. Soc.*, **89**, 219-221, doi: 10.1175/BAMS-89-2-219. [Link]
- Knabb, R. D., J. R. Rhome, and D. P. Brown, 2005: Hurricane Katrina, 23-30 August 2005. Tropical Cyclone

- Report, National Oceanic and Atmospheric Administration, National Weather Service, National Hurricane Center, Miami, Florida, 43 pp.
- Landsea, C. W., J. L. Franklin, C. J. McAdie, J. L. Beven II, J. M. Gross, B. R. Jarvinen, R. J. Pasch, E. N. Rappaport, J. P. Dunion, and P. P. Dodge, 2004: A reanalysis of Hurricane Andrew's intensity. *Bull. Am. Meteorol. Soc.*, **85**, 1699-1712, doi: 10.1175/BAMS-85-11-1699. [[Link](#)]
- Luetlich, R. A. Jr. and J. J. Westerink, 2006: ADCIRC: A parallel advanced circulation model for oceanic, coastal and estuarine waters; users manual for version 45.08. Available online at: http://adcirc.org/document/ADCIRC_title_page.html.
- National Hurricane Center, 2011a: Storm surge maximum envelope of water. Available online at: http://www.nhc.noaa.gov/ssurge/ssurge_meowOverview.shtml.
- National Hurricane Center, 2011b: Storm surge maximum of the maximum. Available online at http://www.nhc.noaa.gov/ssurge/ssurge_momOverview.shtml.
- National Hurricane Center, 2012: NHC archive of hurricane seasons. Available online at <http://www.nhc.noaa.gov/pastall.shtml>.
- Parker, B. B., 1991: Sea level as an indicator of climate and global change. *Mar. Tech. Soc. J.*, **25**, 13-24.
- Powell, M. D. and T. A. Reinhold, 2007: Tropical cyclone destructive potential by integrated kinetic energy. *Bull. Am. Meteorol. Soc.*, **88**, 513-526, doi: 10.1175/BAMS-88-4-513. [[Link](#)]
- Rappaport, J. and J. D. Sachs, 2003: The United States as a coastal nation. *J. Econ. Growth*, **8**, 5-46, doi: 10.1023/A:1022870216673. [[Link](#)]
- Resio, D. T., J. L. Irish, and M. A. Cialone, 2009: A surge response function approach to coastal hazard assessment - Part 1: Basic concepts. *Nat. Hazards*, **51**, 163-182, doi: 10.1007/s11069-009-9379-y. [[Link](#)]
- Salisbury, M. B., S. C. Hagen, D. Coggin, P. Bacopoulos, J. Atkinson, and H. Roberts, 2011: Unstructured mesh development for the Big Bend Region (Florida). *Fla. Watershed J.*, **4**, 11-14.
- Simpson, R. H., 1974: The hurricane disaster-potential scale. *Weatherwise*, **27**, 169-186, doi: 10.1080/00431672.1974.9931702. [[Link](#)]
- Slinn, D. N., M. C. Robinson, G. Fujita, and L. C. Charles, 2011: Wave modeling for the east Florida panhandle flood study. *Fla. Watershed J.*, **4**, 15-21.
- SWAN Team, 2010: SWAN cycle III; users manual for version 40.81. Available online at <http://www.swan.tudelft.nl>.
- Toro, G., S. C. Hagen, J. Atkinson, and C. Reed, 2011: Production runs for the Big Bend Region of Florida. *Fla. Watershed J.*, **4**, 28-35.
- Walton, T. L. Jr., 2007: Projected sea level rise in Florida. *Ocean Eng.*, **34**, 1832-1840, doi: 10.1016/j.oceaneng.2007.02.003. [[Link](#)]
- Zervas, C., 2001: Sea level variations of the United States 1854-1999. NOAA Technical Report NOS CO-OPS 36, National Oceanic and Atmospheric Administration, US Department of Commerce, National Ocean Service, Silver Spring, Maryland, 194 pp.
- Zhang, K., 2011: Analysis of non-linear inundation from sea-level rise using LIDAR data: A case study for South Florida. *Clim. Change*, **106**, 537-565, doi: 10.1007/s10584-010-9987-2. [[Link](#)]